



# Real-Time Simulator of DTC–FOC-Based DFIG During Voltage Dip and LVRT

Kiran Kumar Jaladi<sup>1</sup>  · Kanwarjit Singh Sandhu<sup>1</sup> · Parimala Bommala<sup>1</sup>

Received: 30 October 2018 / Revised: 9 December 2019 / Accepted: 17 December 2019 / Published online: 1 January 2020  
© Brazilian Society for Automatics–SBA 2020

## Abstract

This paper proposes the decoupling control of direct torque control (DTC) and field orient control (FOC) for doubly fed induction generator (DFIG)-based wind energy system (WES). The proposed technique reduces the transient of system during low voltage ride through (LVRT) as well as voltage dip (VD) with out auxiliary circuit. The combined DTC–FOC regulates both rotor and grid side converters (RGSCs). In particular, DTC controls the generator speed, torque and rotor flux; similarly, FOC regulates the capacitor link voltage and power quality of grid during LVRT and VD. The linear controller is unable to control the nonlinearities of system dynamics with respect to time. Further, the proposed technique is analyzed with sliding mode control (SMC) and conventional controllers independently. The proposed DTC–FOC aims to improve the performance of transient and dynamic behavior of DFIG-based WES during LVRT and VD. It is also tested in real-time environment at 7.5 hp as well as MATLAB/SIMULINK of 5.5 kW rating.

**Keywords** Doubly fed induction generator · Wind energy system · Sliding mode control · Low voltage ride through · Voltage dip · Direct torque control

## 1 Introduction

Recent trends suggested that wind energy (WE) is one of the major contributors and rapidly growing among all renewable energy resources. In WE, doubly fed induction generator (DFIG) is the most efficient machine in contrast to permanent magnetic synchronous machine (PMSM), because of its speed control flexibility, more efficiency and lesser rating of converters. Generally, the rotor circuit connected through a back-to-back power converters and stator of DFIG is directly fed to the utility grid (Firouzi and Gharehpetian 2018). DFIG-based WE (DFIGWE) systems are sensitive toward continuous variation of wind velocity and disturbances in grid.

However, DFIGWE is penetrating toward voltage sags and fault ride through (FRT) due to fact that both stator and rotor are directly fed to DFIG through back-to-back converters. Many researchers proposed different methods to solve low voltage ride through (LVRT), VD and FRT problem with external protection circuits (Rashid and Ali 2017). The main problems associated with voltage sags are abrupt changes in generator speed, rotor current transients and sever transients of DC-link capacitor voltage. Disconnect of the wind turbines (WT) from the power grid during LVRT and VD causes waste of energy. The stop and start of wind power generator may cause a big fluctuation, which may cause power system instability (Alsmadi 2018).

Because such problems can be eliminated by using enriched controllers like field orient control (FOC), direct torque control (DTC) and direct power control (DPC) techniques are used to control the utility grid as well as wind speeds (Yong Kang and Chen 2003). FOC is the most adapted technique for DFIGWE systems, and it improves the performance of steady-state condition and also attains lower switching frequency. But FOC has it own drawbacks, which are plurality of current control loops, dependency on machine parameters and coordinate transformation. These limitations are effectively taken over by DTC technique. DTC is simple

✉ Kiran Kumar Jaladi  
202.kiran@nitkkr.ac.in

Kanwarjit Singh Sandhu  
kjssandhu@rediffmail.com

Parimala Bommala  
parimala.bomala@gmail.com

<sup>1</sup> Department of Electrical Engineering, National Institute of Technology, Kurukshetra, Haryana, India

in structure compared to FOC technique, but DTC has its own disadvantage of variable sampling frequency. Because hysteresis loops are used in conventional DTC, thus to attain a constant sampling frequency, a space vector modulation (SVM) can be used instead of switching table and hysteresis loops (Arbi et al. 2009; Jaladi and Sandhu 2018, 2019a, b). SVM-based DTC-DFIG may be adopted to get quick response and smooth variation torque and flux.

This paper has made a significant contribution to DTC-FOC-based DFIGWE (DTC-FOC-DFIGWE). DTC-FOC includes combination of FOC and DTC. DTC is applied to rotor side converter (RSC) to control the rotor flux and generator speed. It also controls the both active and reactive power components indirectly, whereas FOC is applied to grid side converter (GSC) to control the capacitor link voltage and also improve the power quality of utility grid (Chang and Kong 2017). The control of DTC and FOC is decoupling to each other. In particular, DTC-FOC takes over problem related to voltage sag, LVRT and FRT. Using DTC-FOC, the problems related to DC voltage transients and rotor currents are controlled within permissible limits by proper designing of proportional and integral (PI) controllers gains and it also minimizes the torque and current ripples. DTC-FOC-DFIGWE does not require any auxiliary protection circuit (Li et al. 2018; Yang et al. 2017; Jaladi 2019; Jaladi and Sandhu 2019), and it means the complexity of the control scheme is reduced during abnormal grid conditions. Because nonlinearity in control scheme PI suffers from settling time torque and current ripples. The solution to the nonlinearities is by using nonlinear controllers like fuzzy, neural network (NN), adaptive neuro-fuzzy inference system (ANFIS) and sliding mode control (SMC).

It has been proved that SMC is a very convenient way to improve the DFIG transients, and it is very robust under a wide range of machine parameters, LVRT and VD of utility grid. The controller of the DFIG wind turbine under SMC ensures cancelation of electromechanical coupling without introducing additional modes. Moreover, this control scheme introduces additional damping which is amenable to reduce local oscillations and an overall better performance than the classical controller DTC-FOC (Zhu et al. 2018; Haidar et al. 2017). SMC has been comprehensive not only in the sense that it encompasses both the RGSCs but also in the sense that it has been applied to cases of multi-machine power systems. Moreover, a wide range of operating scenarios was considered and the new control strategy based on SMC, which is nonlinear, showed a very robust performance. A case in point is the generator model and control strategies for the study of small-signal stability of a wind turbine generator connected to an equivalent grid.

Therefore, this paper includes the analysis and design of SMC and PI-based DTC-FOC of DFIG to be employed in a WES. In Sects. 2 and 3, the transient and dynamic model-

ing of the DFIG is presented. Section 3 includes the control strategy for the DTC-FOC. Sections 4 and 5 demonstrate the effectiveness of the proposed control scheme on a 5.5 kW DFIG model using real-time simulator (RTS)-based OPAL-RT and MATLAB/SIMULINK.

## 2 Modeling of DFIG

The equivalent circuit model is based on the basic equations of the asynchronous machine. These equations are expressed in a reference frame aligned with synchronous speed, taking positive currents. The machine equations can be written in the synchronous rotating  $d-q$  reference frame as follows (Zhu et al. 2017):

$$\begin{aligned}
 V_{qs} &= \frac{d\phi_{qs}}{dt} + \omega\psi_{ds} + R_s i_{qs} \\
 V_{ds} &= \frac{d\phi_{ds}}{dt} + \omega\psi_{qs} + R_s i_{ds} \\
 V_{qr} &= \frac{d\phi_{qr}}{dt} + (\omega - \omega_r)\phi_{dr} + R_r i_{qr} \\
 V_{dr} &= \frac{d\phi_{dr}}{dt} + (\omega - \omega_r)\phi_{qr} + R_r i_{dr} \\
 \phi_{qs} &= (L_{ls} + L_m)i_{qs} + L_m i_{qr} \\
 \phi_{ds} &= (L_{ls} + L_m)i_{ds} + L_m i_{dr} \\
 \phi_{qr} &= (L_{lr} + L_m)i_{qr} + L_m i_{qs} \\
 \phi_{dr} &= (L_{lr} + L_m)i_{dr} + L_m i_{ds} \\
 T_e &= \frac{3p}{2}(\phi_{qr}i_{dr} - \phi_{dr}i_{qr})
 \end{aligned} \tag{1}$$

The active and reactive powers in stator part and rotor part could be calculated as follows:

$$\begin{aligned}
 P_s &= \frac{3}{2}(V_{ds}i_{ds} + V_{qs}i_{qs}) \\
 Q_s &= \frac{3}{2}(V_{qs}i_{ds} - V_{ds}i_{qs})
 \end{aligned} \tag{2}$$

## 3 Transient Behavior of DFIG

The transient behavior of DFIG during LVRT by taking induction motor model by considering rotor voltages in synchronous reference frame is shown in Fig. 1. Equation (1) is rewritten by choosing all parameters referring to stator side (Wang et al. 2017; Djilali et al. 2018).

$$\begin{aligned}
 \vec{V}_s &= R_s \vec{i}_s + \frac{d\vec{\phi}_s}{dt} \\
 \vec{V}_r &= R_r \vec{i}_r + \frac{d\vec{\phi}_r}{dt} - j\omega_r \vec{\phi}_r
 \end{aligned}$$

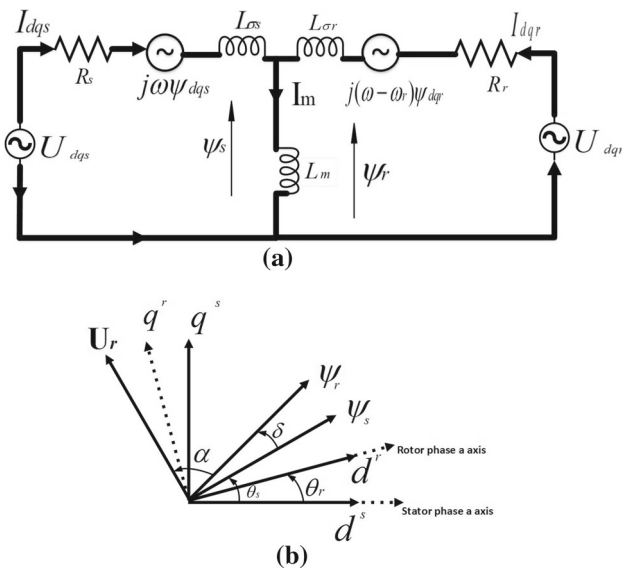


**Fig. 1** Induction motor equivalent circuit in the synchronous reference frame and vector diagram of stator flux orientation vector diagram

$$\begin{aligned}
 \vec{\phi}_s &= L_s \vec{i}_s + L_m \vec{i}_r \\
 \vec{\phi}_r &= L_r \vec{i}_r + L_m \vec{i}_s \\
 \vec{i}_s &= \frac{\vec{\phi}_s - L_m \vec{i}_r}{L_s}, \vec{\phi}_r = \frac{L_m}{L_s} \vec{\phi}_s + \sigma \vec{i}_r L_r
 \end{aligned} \tag{3}$$

From above Eq. (3) written as

$$\begin{aligned}
 \vec{V}_r &= \vec{V}_{ro} + \left[ R_r + \sigma L_r \left( \frac{d}{dt} - j\omega_r \right) \right] \vec{i}_r \\
 \vec{V}_{ro} &= \frac{L_m}{L_s} \left( \frac{d}{dt} - j\omega_r \right) \vec{\psi}_s.
 \end{aligned} \tag{4}$$

At the instant of voltage dip, the forced stator flux and voltage are calculated using both post-fault and pre-fault. The resultant no-load voltage of rotor is given by

$$\vec{V}_{r0} = (1-p) \cdot V \cdot \frac{L_m}{L_s} \cdot s \cdot e^{j\omega_s t} - \frac{L_m}{L_s} \left( \frac{1}{T_s} + j\omega_s \right) \cdot p \cdot \frac{\vec{u}}{j\omega_s} \cdot e^{T_s} \tag{5}$$

### 4 DTC–FOC Control

The proposed technique is a combined control of FOC and DTC. To control the capacitor link voltage,  $dq$ -axis grid currents and also enhancement power quality of grid, FOC is applied to GSC. The feedback control loops of upper portion of Fig. 2 include the three-phase grid voltages and currents, DC-link voltage. Similarly, in the lower portion of Fig. 2, feedback loops include the three-phase rotor voltage and currents. However, DTC is applied to RSC, and it indirectly

controls both active and reactive power, direct control of torque and rotor flux. The block diagram of DTC–FOC-based DFIGWES is shown in Fig. 2

Based on the dynamic model of DFIG (Eq. (1)), the relation between rotor flux and  $d$ -axis rotor voltage equation is given by

$$\begin{aligned}
 &\left( \frac{R_s L_r - R_r L_s k k_1}{R_r} \frac{d}{dt} \right) V_{dr} \\
 &= \left( \frac{R_s R_r}{R_r L_s k k_1} + \frac{R_s L_r L_m k_1}{R_r L_s} \right) \frac{d}{dt} \phi_{dr} \\
 &\quad + \left( \frac{R_s L_r k k_1}{R_r} \frac{d^2}{dt^2} \right) \phi_{dr} \\
 &\quad + \left( \frac{R_s L_r k k_1}{R_r} (\omega - \omega_r) \frac{d}{dt} - \left( \frac{R_s L_r (\omega - \omega_r)}{R_r L_s k k_1} \right) \right) \phi_{qr} \\
 &\quad - R_s L_r k_1 V_{ds} - R_s L_r k_1 k i_{qr}
 \end{aligned} \tag{6}$$

where  $k = \frac{R_r L_m}{R_s L_r}$ ,  $k_1 = \frac{L_m^2 - L_s L_r}{L_m}$  and  $k_2 = \frac{L_s L_r - L_m^2}{L_s}$ ,  $k_3 = R_r L_s + R_s L_r$ , the transfer function of rotor flux to  $d$ -axis rotor voltage obtained by applying Laplace transform of Eq. (6) as follows:

$$\frac{\phi_{dr}}{V_{dr}} = \frac{R_s L_r + (L_s L_r - L_m^2) s}{(L_s L_r - L_m^2) s^2 + \left( \frac{R_r L_m^2}{L_s} + R_s L_r \right) s + R_s R_r} \tag{7}$$

From Eq. (1), finding the relation between  $q$ -axis rotor current in terms of generator speed termed as by choosing SFO notation

$$i_{qr} = -\frac{2L_s}{3L_m \psi_{ds}} T_e \frac{d\omega_r}{dt} = -\frac{p}{J} \frac{3L_m \psi_{ds}}{2L_s} i_{qr}. \tag{8}$$

Similarly, the relation between electromagnetic torque and rotor  $q$ -axis voltage is found by using Eqs. (1) and (8)

$$\left[ L_s \frac{d}{dt} \right] V_{qr} = \left[ \left( \frac{2L_s}{3L_m \phi_{ds}} \right) \left( \frac{L_s L_r - L_m^2}{L_m} \right) \frac{d^2}{dt^2} + \frac{2L_s k_3}{3L_m \phi_{ds}} \frac{d}{dt} + L_m \phi_{ds} \frac{p}{J} \right] T_e \tag{9}$$

Taking the Laplace transform of Eq. (9) gives the open-loop transfer function of torque and  $q$ -axis rotor voltage.

$$\frac{T_e}{V_{qr}} = \frac{L_s s}{\frac{2L_s}{3\phi_{ds}} \left( \frac{L_s L_r - L_m^2}{L_m^2} \right) s^2 + \frac{2L_s k_3}{3L_m \phi_{ds}} s + L_m \phi_{ds} \frac{p}{J}} \tag{10}$$

Using Eqs. (7) and (9), the PI controller is designed by using symmetry criteria method (SCM) to study the pole-zero mapping of rotor side controller. From Eq. (7), the rotor flux, the gain value  $s$  between 1 and 5 the pole are placing in semi-circle in imaginary axis, crossing of gain value 5 give the poles placement of real axis is shown in Fig. 3. Similarly,



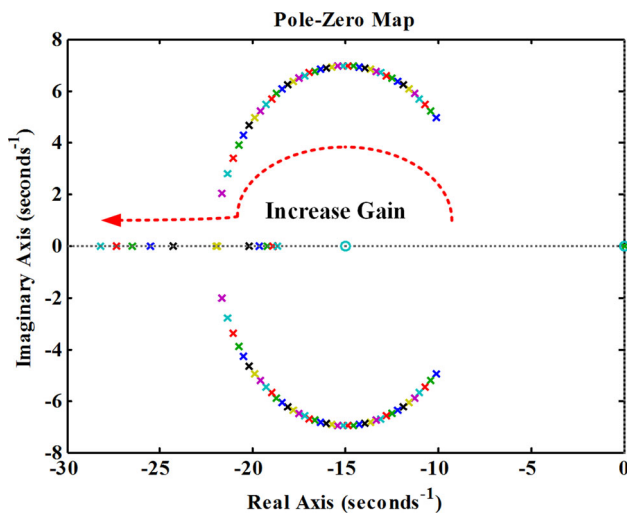


Fig. 5 Zero-pole mapping of torque during gain variation 5–10

power generation. It was found that the best control strategy was: (i) to apply SMC in the machine side converter to control the rotor voltage in order to operate the wind turbine at optimum efficiency, at the desired power factor; (ii) to apply SMC in the grid side converter to maximize the damping of electromechanical oscillations by drawing on its reactive power capability. The control law was derived using a defined Lyapunov function.

From Eq. (1), the dynamic modeling of DFIG, electromagnetic torque,  $q$ -axis rotor voltage and rotor flux that can be written in stator flux orientation (SFO) is given by

$$\begin{aligned} T_e &= -\frac{3}{2} \frac{L_m}{L_s} \phi_{ds} i_{qr} \\ V_{qr} &= R_r i_{qr} + \frac{d\phi_{qr}}{dt} - (\omega_s - \omega) \phi_{dr} \\ \phi_{qr} &= L_r i_{qr} + L_m i_{qs} \end{aligned} \tag{11}$$

The simplified torque equation (Eq. (11)) is rewritten in  $q$ -axis components as

$$\begin{aligned} T_e &= \left[ \frac{3}{2} (1 - \sigma) i_{qs} - \frac{3}{2} \frac{(1 - \sigma)}{L_m} \phi_{qr} \right] \phi_{ds} \\ \sigma &= 1 - \frac{L_m^2}{L_s L_r} \end{aligned} \tag{12}$$

Torque sliding surface and derivative of torque are given by Eq. (13)

$$\begin{aligned} S_{T_e} &= T_e - T_{ref} \\ \frac{dS_{T_e}}{dt} &= \left[ \frac{3}{2} a \left\{ -V_{qr} + i_{qr} \cdot \frac{L_r}{T_r} + (\omega_s - \omega) \phi_{dr} + \frac{(1 - \sigma)}{L_m} L_r \right\} \right] \cdot \phi_{ds} \\ A_1 &= \left[ \frac{3}{2} a \left\{ -V_{qr} + i_{qr} \cdot \frac{L_r}{T_r} + \frac{(1 - \sigma)}{L_m} L_r \left( \frac{V_{qs} - R_s i_{qs} - \phi_{ds} \omega_s}{L_r} \right) \right\} \right] \cdot \phi_{ds} \end{aligned}$$

$$a = \frac{1 - \sigma}{\sigma L_m} \tag{13}$$

Using Eqs. (11) and (13), take the similarly notation for rotor flux using

$$\begin{aligned} S_{\phi_r} &= \phi_r - \phi_{ref} \\ \frac{dS_{\phi_r}}{dt} &= b \frac{di_{dr}}{dt} \\ b &= \frac{K}{s + T_r} \end{aligned} \tag{14}$$

The derivative of rotor flux is given by

$$\begin{aligned} \frac{dS_{\phi_r}}{dt} &= b \left[ cV_{dr} - \frac{1}{\sigma T_r} i_{dr} + c\phi_{qr}(\omega_s - \omega) - aV_{ds} \right] \\ \frac{dS_{\phi_r}}{dt} &= b \left[ A_2 - aV_{ds} + aR_s i_{ds} - b_4 \omega_s \phi_{qs} \right] \\ A_2 &= cV_{dr} - \frac{1}{\sigma T_r} i_{dr} + c\phi_{qr}(\omega_s - \omega) \quad c = \frac{1}{\sigma L_r} \end{aligned} \tag{15}$$

where  $\phi_r, T_e$  are the actual values and  $\phi_{ref}, T_{ref}$  are the corresponding reference values of rotor flux and electromagnetic torque, respectively. Torque and flux dynamic slinging surface are given by

$$\begin{aligned} \frac{dS_{\phi_r}}{dt} &= -K \text{sign}(S_{\phi_r}) - G S_{\phi_r} \\ \frac{dT_e}{dt} &= -K \text{sign}(S_{T_e}) - G S_{T_e} \\ V_{dr} &= \frac{-K \text{sign}(S_{T_e}) - G S_{T_e} - A_1}{\frac{3}{2} a (\omega_s - \omega) \phi_{dr}} \\ V_{qr} &= \frac{K \text{sign}(S_{\phi_r}) + G S_{\phi_r} + bA_2 + baR_s i_{ds} + abV_{ds}}{a\omega_s} \end{aligned} \tag{16}$$

Convergence of rotor flux and torque is improved by designing  $G S_{T_e}, G S_{\phi_r}$  and also choosing positive values of  $G$  and  $K$ . To get the robustness of SMC and eliminating estimated problems, Eq. 16 is modified as

$$\begin{aligned} V_{dr} &= \frac{K \text{sign}(S_{T_e}) - G S_{T_e} - \bar{A}_1}{\frac{3}{2} \bar{a} (\omega_s - \omega) \phi_{dr}} \\ V_{qr} &= \frac{K \text{sign}(S_{\phi_r}) + G S_{\phi_r} + b\bar{A}_2 + baR_s i_{ds} + abV_{ds}}{\bar{a}\omega_s} \end{aligned} \tag{17}$$

To examine the stability by choosing Lyapunov function  $V$ , the first derivative of  $V$  is given by

$$\begin{aligned} V &= \frac{1}{2} S_{T_e}^2 + \frac{1}{2} S_{\phi_r}^2 \\ \dot{V} &= S_{T_e} \cdot \frac{dS_{T_e}}{dt} + S_{\phi_r} \cdot \frac{dS_{\phi_r}}{dt} \end{aligned} \tag{18}$$

Substituting Eqs. (13) and (15) in the first derivative of Lyapunov function

$$\begin{aligned} \dot{V} = & S_{T_e} \left[ A_1 + \frac{a}{a} (-K \text{sign}(S_{T_e}) - G S_{T_e} - \overline{A}_1) \right] \\ & + S_{\phi_r} \left[ \overline{bA}_2 + ba R_s i_{ds} - ba V_{ds} \right. \\ & \left. - \frac{a}{a} (K \text{sign}(S_{\phi_r}) + G S_{\phi_r} + g \overline{A}_2 + ba R_s i_{ds} + ba V_{ds}) \right] \end{aligned}$$

or

$$\begin{aligned} \dot{V} = & \left( A_1 - \frac{a}{a} \overline{A}_1 \right) S_{T_e} + \left( bA_2 - \frac{a}{a} \overline{bA}_2 \right) S_{\phi_r} \\ & - \frac{a}{a} G (S_{T_e}^2 + S_{\phi_r}^2) \\ & + S_{\phi_r} \left[ ab R_s i_{ds} \left( 1 - \frac{a}{a} \right) - ba V_{ds} \left( 1 + \frac{a}{a} \right) \right] \end{aligned} \quad (19)$$

The time differentiation of Lyapunov function is positive if

$$K < \frac{a}{a} \left[ \left( A_1 - \frac{a}{a} \overline{A}_1 \right) S_{T_e} + \left( bA_2 - \frac{a}{a} \overline{bA}_2 \right) S_{\phi_r} \right] \quad (20)$$

Better robustness of both rotor flux and torque is achieved by taking the greater positive value of K.

### 6 Results and Discussion

The proposed technique of a grid-connected DFIG-based WES with SMC and PI controllers is carried out in MATLAB/Simulink environment. The DTC–FOC control method generates pulses to both RSC and GSC in order to achieve less oscillations of capacitor link voltage and rotor speed smoothing of DFIG under different utility grid conditions like LVRT and VD. A stepwise wind speed profile has been applied with minimum and maximum wind speed values in order to test the system under different rotor speed conditions (motoring and generating mode of operation). LVRT and VD profile was applied to examine the system performance under more realistic wind speed profile. In this paper, DFIG is chosen at a rating of 5.5kW and its parameters are listed in Tables 1 and 2. The simulation results for proposed and PI-based DTC–FOC DFIG WES are shown in Figs. 6, 7, 8 and 9. These results represents the stator voltages ( $V_s$ ), active ( $P_s$ ) and reactive ( $Q_s$ ) power of stator, generating speed ( $N_r$ ), torque ( $T_e$ ), capacitor link voltage ( $V_{dc}$ ), stator ( $I_{sabc}$ ) and rotor ( $I_r abc$ ) currents, and magnitude of rotor flux ( $\phi_r$ ). The reference and desired values are shown in Figs. 6, 7, 8 and 9. The comparative PI and SMC LVRT results are presented in Figs. 6, 7; from Fig. 6a, LVRT of stator voltage initiation is at  $t = 1.0$  s and clear at  $t = 1.6$  s. During LVRT, the active power and reactive power oscillations are more in PI in contrast to SMC as shown in Fig. 6b, c. In a similar manner, Fig. 6e, f shows predominant transients of torque and capacitor link voltages improved in SMC compared to PI. The generator speed ripples and settling time of proposed technique which are better than those

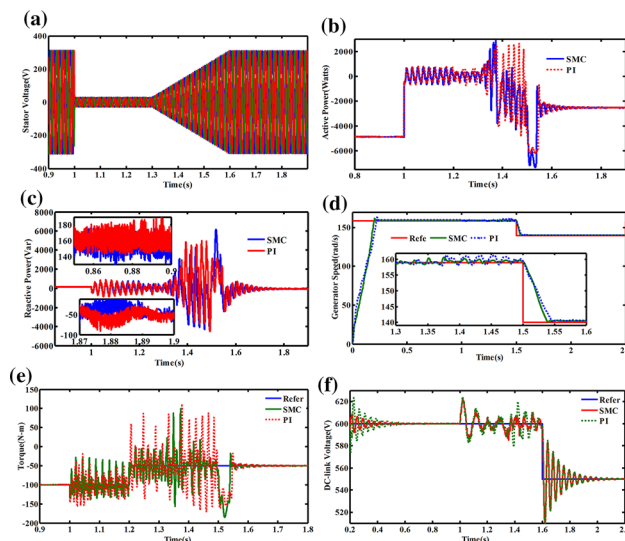


Fig. 6 LVRT simulation results with SMC and PI DFIG-based WES a stator voltage, b active power, c reactive power, d generator speed, e torque, and f capacitor voltage

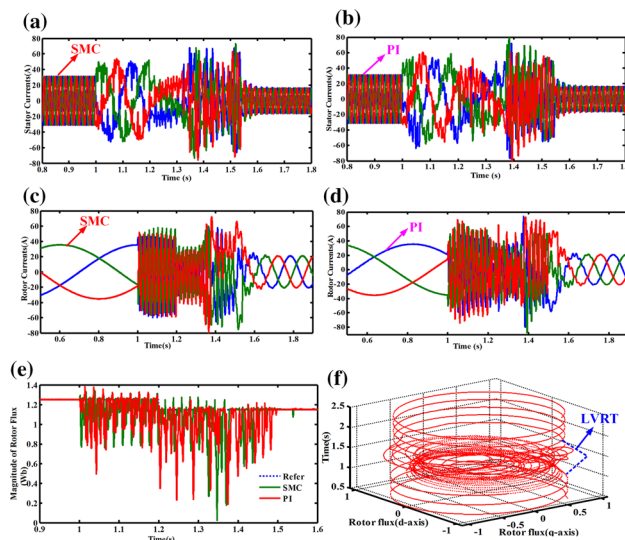
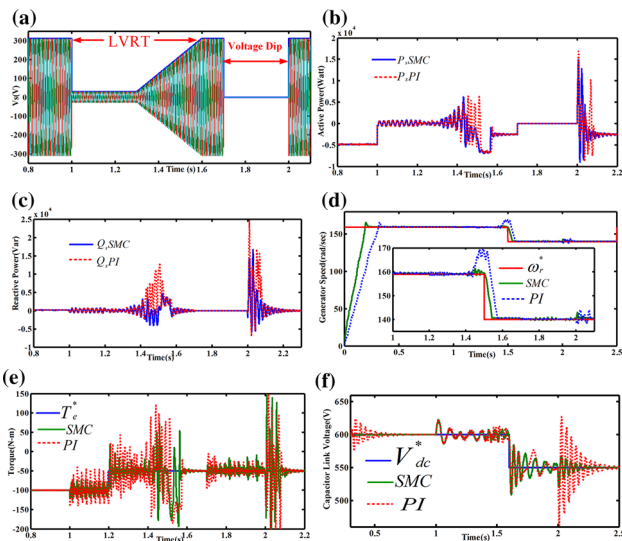
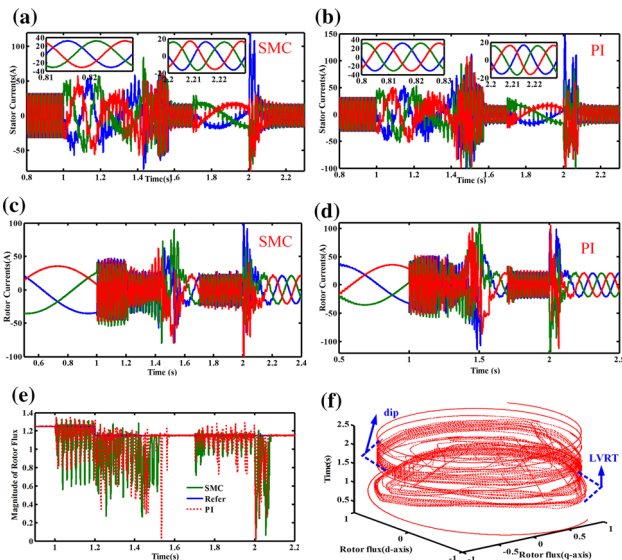


Fig. 7 LVRT simulation results with SMC and PI DFIG-based WES a, b stator currents; c, d rotor currents; e rotor flux, f dq-axis rotor flux

of PI during LVRT are shown in Fig. 6d. From Fig. 6, we conclude that the actual values of torque and rotor speed are tracking its reference values, respectively. Similarly, Fig. 7 shows the stator currents, rotor currents, magnitude of rotor flux and dq-axis rotor flux. From Fig. 7a, b, the oscillations and transients of stator currents are better in proposed SMC compared to PI. From Figure 7c, d, rotor transients are more predominant in PI compared to SMC. The actual rotor flux follows the reference, but more transients presented in PI contrast to SMC and also rotor flux within the permissible limits. For better understanding of rotor flux during the LVRT is shown in Fig. 7f.



**Fig. 8** Combined LVRT and VD simulation results with SMC and PI DFIG-based WES **a** stator voltage, **b** active power, **c** reactive power, **d** generator speed, **e** torque, and **f** capacitor voltage



**Fig. 9** Combined LVRT and VD simulation results with SMC and PI DFIG-based WES **a**, **b** stator currents, **c**, **d** rotor currents, **e** rotor flux, **f**  $dq$ -axis rotor flux

Figures 8 and 9 show the comparison simulation results for both SMC and PI during LVRT with VD. The conditions are the same for the above-said LVRT, but in addition to VD initiate at 1.7s and clear at 2s. Stator voltage is shown in Fig. 8a; the active power and reactive power transients are more in PI during clearing period of LVRT and VD compared to SMC as shown in Fig. 8b, c. The oscillations and ripples of active and reactive power are more in LVRT and zero for during voltage dip; this is due to the fact that magnitude of stator voltages is zero. Figure 8d shows the generator speed of both actual and reference for SMC and PI. Speed

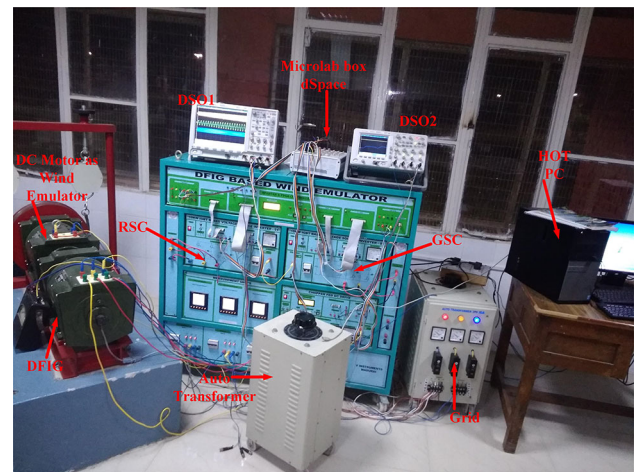


**Fig. 10** Experimental schematic diagram of HC-based DFIGWES

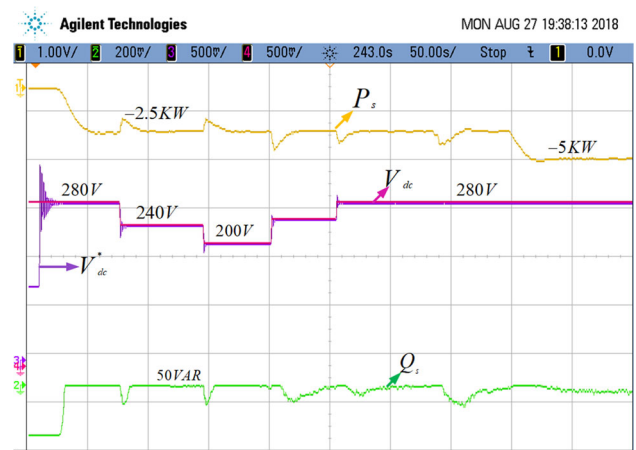


**Fig. 11** DFIG experimental validation of step change in both speed and DC-link voltage

transients are more in PI during LVRT, and also more ripples are present in VD compared to SMC. The torque and capacitor link voltage oscillations and ripples are improved in the proposed SMC technique compared to SMC shown in Fig. 8e, f. Similarly, in Fig. 9a–d, rotor and stator transients are more predominant in PI compared to SMC during LVRT and VD. The reference and actual rotor flux follow each other, but less transients are presented in SMC in contrast to PI and also rotor flux within the permissible limits. For better understanding, rotor flux during the LVRT and VD is shown in Fig. 9f. From Figs. 6, 7, 8 and 9, we conclude that the actual values of rotor flux, generator speed, capacitor link voltage and electromagnetic follow the corresponding reference values in steady-state condition as well as LVRT and VD for both controllers, but in PI produce the more oscillations and transients during VD and LVRT grid conditions.

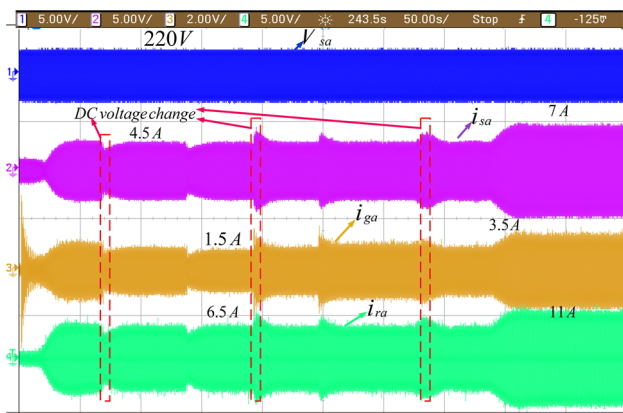


**Fig. 12** DFIG experimental stator phase voltage, stator, grid and rotor current during step change in speed, torque and DC-link voltage

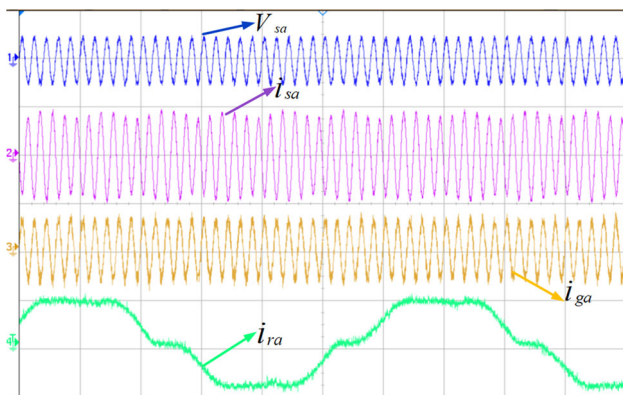


**Fig. 13** Zooming portion of Fig. 12

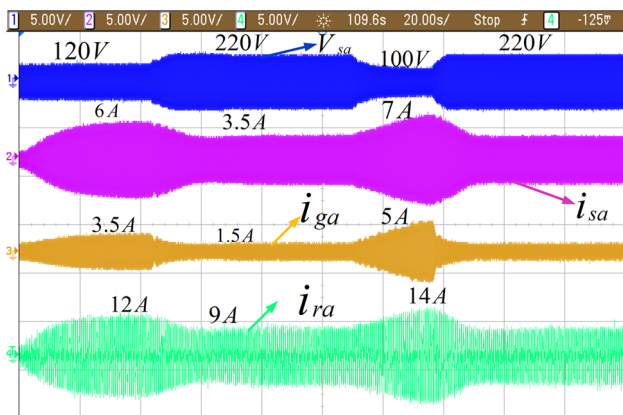


**Fig. 14** DTC-FOC experimental results of stator, grid and rotor current during VD and LVRT

### 7 Experimental Results

The experimental prototype details are shown in Fig. 10. It includes the generator motor setup, back-to-back converters, host PC, dSPACE microlab box, autotransformers, sensors and digital signal oscilloscopes (DSO). Here, the HC algorithm is developed in FPGA-based DS1202. Figure 11 shows

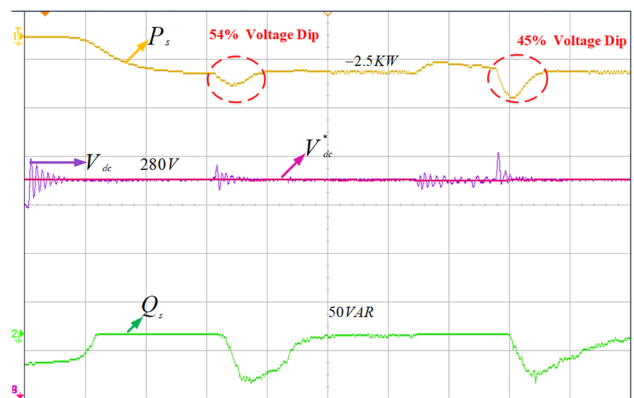


**Fig. 15** DTC-FOC experimental results of active and reactive power, and capacitor link voltage during VD and LVRT

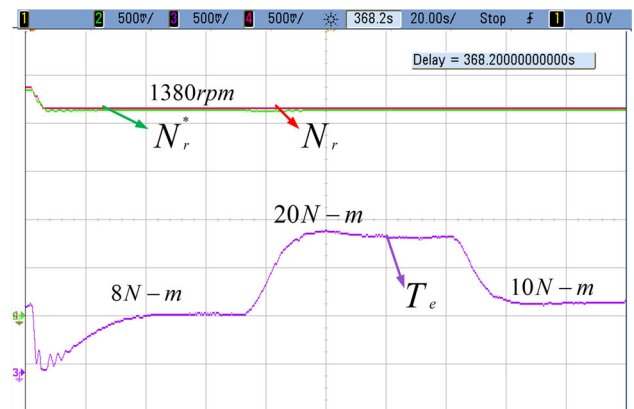


**Fig. 16** DTC-FOC experimental results of rotor speed, torque, stator and rotor current during step change of both torque and speed

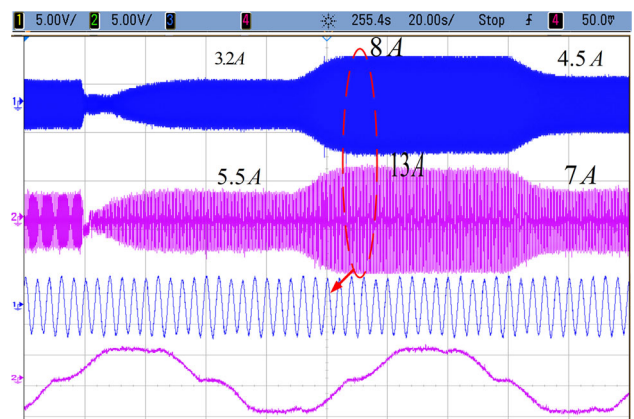


**Fig. 17** DTC-FOC experimental results of stator and rotor current during step change of both torque and speed

the step change of torque, capacitor link voltage, active and reactive powers. The control technique tracks the reference DC voltage and also produces less transients of both active ( $-2.5\text{ kW}$ ) and reactive ( $50\text{ var}$ ) powers under steady-state condition. The power transients are due to step change in capacitor link voltage and generator speed. The oscillation



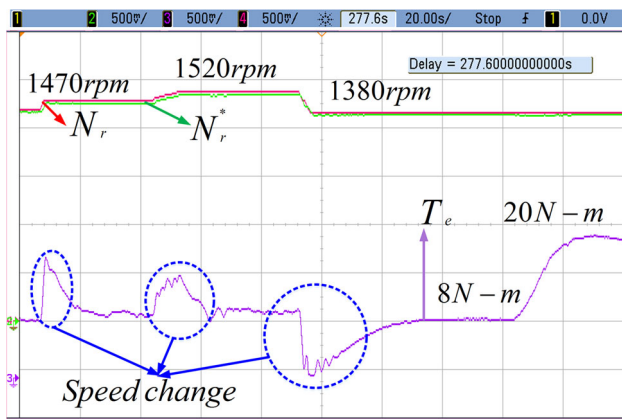


**Fig. 18** DTC-FOC experimental results of rotor speed, torque, stator and rotor current during steeply change of both torque and speed

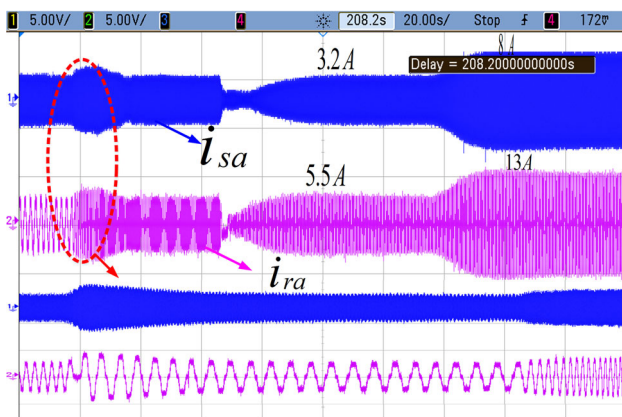


**Fig. 19** DTC-FOC experimental results of stator and rotor current during steeply change of both torque and speed

of active and reactive powers is between  $-2$  to  $-2.2$  kW and  $-100$  to  $50$  var, also more settling time required. The condition of Fig. 12 shows corresponding conditions of Fig. 11; it shows the stator voltage, currents of stator, grid and rotor. The step change of torque corresponding to stator phase voltage  $220$  V, stator, grid and rotor currents of in between  $5.5$ – $7.5$  A,  $2.5$ – $4.5$  A and  $8$ – $11$  A. The zooming portion of corresponding Fig. 12 is given in Fig. 13. The results of the combined VD and LVRT analysis of the proposed DFIG-based WES during  $13$  N-m are seen in Figs. 14 and 15. The VD of grid  $0.54$  and  $0.45$  times rated phase voltage of time interval of  $0$ – $50$  s and  $110$ – $140$  s respectively. Figure 14 shows the currents of stator, grid and rotor: during VD, the current transients of stator ( $7.5$  A), grid ( $4.5$  A) and rotor ( $13$  A), and similarly during LVRT, current transients of stator ( $9$  A), grid ( $5.5$  A) and rotor ( $14$  A), respectively. The details of Fig. 15 describe the active power, reactive power, actual and reference of capacitor link voltage: transients of active ( $-2.5$  to  $-3.2$  kW) and reactive ( $50$  var to  $-200$  var) powers for VD of grid and during LVRT the active ( $-2.5$  to  $-4$  kW) and reactive ( $50$  var to  $-150$  var) powers, respectively. Similarly, Fig. 15 shows the

**Table 1** Simulation rating of DFIG

Parameters	Values
Rated power	5.5 kW
Rated frequency	50 Hz
Stator voltage ( $u_s$ )	380 V
Stator resistance ( $R_s$ )	$0.719 \Omega$
Rotor resistance ( $R_r$ )	$0.655 \Omega$
Stator leakage inductance ( $L_{\sigma s}$ )	$8.0546$ mH
Rotor leakage inductance ( $L_{\sigma r}$ )	$8.076$ mH
DC-link capacitance ( $C$ )	$0.015$ F
DC-link maximum voltage ( $U_{dc}$ )	$1200$ V
Filter resistance of grid ( $R_g$ )	$0.1 \Omega$
Filter inductance of grid ( $L_g$ )	$1.3$ mH
Pole pairs $p$	2
Base wind speed ( $V_w$ )	$14$ m/s

**Table 2** HIL rating of DFIG

Parameters	Values
Rated power	7.5 hp
Rated frequency	50 Hz
Stator voltage ( $u_s$ )	440 V
Stator resistance ( $R_s$ )	$1 \Omega$
Rotor resistance ( $R_r$ )	$1.1 \Omega$
Stator leakage inductance ( $L_{\sigma s}$ )	$0.0103$ H
Rotor leakage inductance ( $L_{\sigma r}$ )	$0.0105$ mH
DC-link capacitance ( $C$ )	$0.000220$ F
DC-link maximum voltage ( $U_{dc}$ )	$320$ V
Filter resistance of grid ( $R_g$ )	$0.1 \Omega$
Filter inductance of grid ( $L_g$ )	$2$ mH
Pole pairs $p$	2
DC motor as wind emulator	7.5 hp

actual capacitor link voltage tracking the reference DC-link voltage, transient of capacitor link voltages during VD ( $270$  V to  $290$  V) and LVRT ( $275$  V to  $298$  V), respectively.

Figures 16, 17, 18 and 19 show stator and rotor currents during step change of both torque and rotor speed: the step change of torque ( $8$  N-m,  $20$  N-m at  $72$  s and  $10$  N-m at  $145$  s) and rotor speed ( $1520$  rpm at  $5$  s and  $1380$  rpm at initial), respectively. Figure 16 shows the constant rotor speed and step change of torque, and corresponding currents of both stator ( $3.2$  A,  $8$  A and  $4.5$  A) and rotor ( $5.5$  A,  $13$  A and  $7$  A) are shown in Fig. 17. Figure 18 shows the steep change of both rotor speed ( $1470$  rpm at  $8$  s,  $1520$  rpm at  $52$  s,  $1380$  rpm at  $114$  s and initial  $1430$  rpm) and torque. Transient of torque at the instant of speed change between  $8$ – $15$  N-m,  $8$ – $14$  N-m and  $8$ – $0$  N-m. The current oscillations of better response are during step change of rotor speed. The corresponding numer-

ical values are shown in respective figures. The proposed SMC-based DTC–FOC controller gives better performance during both steady-state and dynamic conditions.

## 8 Conclusion

The decoupling control of SMC-based DTC and FOC for DFIG-based WES shows better improved performance compared to PI. SMC shows reduced transients of stator and rotor currents, capacitor link voltage, torque and generator speed in contrast to PI controller. DTC–FOC technique aims to minimize both the speed and capacitor link oscillations during LVRT and VD. The proposed technique is also verified with HIL. The DTC–FOC method satisfactory conditions is given by

1. The SMC-based DTC–FOC technique shows the reduced ripples of torque, flux, currents and also smoothing of generator speed as compared to PI under ideal grid conditions.
2. The proposed scheme-based SMC shows the better performance of DC-link voltage oscillations, current transients, torque and flux ripples and also smoothing of generator speed as compared to PI during LVRT and VD conditions.

DTC–FOC–DFIG improves the WES performance without any auxiliary circuit up to 3.5kW range during LVRT and VD grid conditions, and it also reduced the ripples under steady-state condition.

## References

- Alsmadi, Y. M., et al. (2018). Detailed investigation and performance improvement of the dynamic behavior of grid-connected DFIG-based wind turbines under LVRT conditions. *IEEE Transactions on Industry Applications*, 54(5), 4795–4812.
- Arbi, J., Ghorbal, M. J. B., Slama-Belkhouja, I., & Charaabi, L. (2009). Direct virtual torque control for doubly fed induction generator grid connection. *IEEE Transactions on Industrial Electronics*, 56(10), 4163–4173.
- Chang, Y., & Kong, X. (2017). Linear demagnetizing strategy of DFIG-based WTs for improving LVRT responses. *The Journal of Engineering*, 2017(13), 2287–2291.
- Djilali, L., Sanchez, E. N., & Belkheiri, M. (2018). Real-time implementation of sliding-mode field-oriented control for a DFIG-based wind turbine. *International Transactions on Electrical Energy Systems*, 28, e2539.
- Firouzi, M., & Gharehpetian, G. B. (2018). LVRT performance enhancement of DFIG-based wind farms by capacitive bridge-type fault current limiter. *IEEE Transactions on Sustainable Energy*, 9(3), 1118–1125.
- Haidar, A. M. A., Muttaqi, K. M., & Hagh, M. T. (2017). A coordinated control approach for DC link and rotor crowbars to improve fault ride-through of DFIG-based wind turbine. *IEEE Transactions on Industry Applications*, 53(4), 4073–4086.
- Jaladi, K. K. (2019). Experimental validation of SMC DTC–VC for DFIG–WECS. *Electrical Engineering*, <https://doi.org/10.1007/s00202-019-00809-6>.
- Jaladi, K. K., & Sandhu, K. S. (2018). DC-link transient improvement of SMC based hybrid control of DFIG–WES under asymmetrical grid faults. *International Transactions on Electrical Energy Systems*, 28, e2633.
- Jaladi, K. K., & Sandhu, K. S. (2019). Real-time simulator based hybrid controller of DFIG–WES during grid faults: Design and analysis. *International Journal of Electrical Power and Energy Systems*, 116, 105545.
- Jaladi, K. K., & Sandhu, K. S. (2019). A new hybrid control scheme for minimizing torque and flux ripple for DFIG-based WES under random change in wind speed. *International Transactions on Electrical Energy Systems*, 29, e2818.
- Jaladi, K. K., & Sandhu, K. S. (2019). Real-Time Simulator based hybrid control of DFIG–WES. *ISA Transactions*, <https://doi.org/10.1016/j.isatra.2019.03.024>.
- Kang, Y., Zhu, P., & Chen, J. (2003). Improved direct torque control performance of induction motor with duty ratio modulation. In *IEEE international electric machines and drives conference 2003* (Vol. 2, pp. 994–998).
- Li, X., Zhang, X., Lin, Z., & Niu, Y. (2018). An improved flux magnitude and angle control With LVRT capability for DFIGs. *IEEE Transactions on Power Systems*, 33(4), 3845–3853.
- Rashid, G., & Ali, M. H. (2017). Nonlinear control-based modified BFCL for LVRT capacity enhancement of DFIG-based wind farm. *IEEE Transactions on Energy Conversion*, 32(1), 284–295.
- Wang, M., Shi, Y., Zhang, Z., Shen, M., & Lu, Y. (2017). Synchronous flux weakening control with flux linkage prediction for doubly-fed wind power generation systems. *IEEE Access*, 5, 5463–5470.
- Yang, S., Zhou, T., Chang, L., Xie, Z., & Zhang, X. (2017). Analytical method for DFIG transients during voltage dips. *IEEE Transactions on Power Electronics*, 32(9), 6863–6881.
- Zhu, D., Zou, X., Deng, L., Huang, Q., Zhou, S., & Kang, Y. (2017). Inductance-emulating control for DFIG-based wind turbine to ride-through grid faults. *IEEE Transactions on Power Electronics*, 32(11), 8514–8525.
- Zhu, D., Zou, X., Zhou, S., Dong, W., Kang, Y., & Hu, J. (2018). Feed-forward current references control for DFIG-based wind turbine to improve transient control performance during grid faults. *IEEE Transactions on Energy Conversion*, 33(2), 670–681.

**Publisher's Note** Springer Nature remains neutral with regard to jurisdictional claims in published maps and institutional affiliations.